HHS Public Access

Author manuscript

*Neuroimage*. Author manuscript; available in PMC 2019 July 01.

Published in final edited form as:

*Neuroimage*. 2018 July 01; 174: 308–316. doi:10.1016/j.neuroimage.2018.03.021.

# Simultaneous quantitative susceptibility mapping and Flutemetamol-PET suggests local correlation of iron and β-amyloid as an indicator of cognitive performance at high age

**J. M. G. van Bergen**[1,*], **X. Li**[2,3], **F. C. Quevenco**[1], **A. F. Gietl**[1,4], **V. Treyer**[1,5], **R. Meyer**[1,4], **A. Buck**[5], **P. A. Kaufmann**[5], **R. M. Nitsch**[1,4], **P. C. M. van Zijl**[2,3], **C. Hock**[1,4], and **P. G. Unschuld**[1,4]

[1]Institute for Regenerative Medicine, University of Zurich, Switzerland [2]The Russell H. Morgan Department of Radiology and Radiological Science, Division of MR Research, The Johns Hopkins University School of Medicine, Baltimore, Maryland, USA [3]F.M. Kirby Research Center for Functional Brain Imaging, Kennedy Krieger Institute, Baltimore, Maryland, USA [4]Hospital for Psychogeriatric Medicine, University of Zurich, Switzerland [5]Department of Nuclear Medicine, University Hospital Zurich and University of Zurich, Zurich, Switzerland

## Abstract

The accumulation of β-amyloid plaques is a hallmark of Alzheimer's disease (AD), and recently published data suggest that increased brain iron burden may reflect pathologies that synergistically contribute to the development of cognitive dysfunction. While preclinical disease stages are considered most promising for therapeutic intervention, the link between emerging AD-pathology and earliest clinical symptoms remains largely unclear. In the current study we therefore investigated local correlations between iron and β-amyloid plaques, and their possible association with cognitive performance in healthy older adults.

116 older adults (mean age 75±7.4 years) received neuropsychological testing to calculate a composite cognitive score of performance in episodic memory, executive functioning, attention, language and communication. All participants were scanned on a combined PET-MRI instrument and were administered T1-sequences for anatomical mapping, quantitative susceptibility mapping (QSM) for assessing iron, and 18F-Flutemetamol-PET for estimating β-amyloid plaque load. Biological parametric mapping (BPM) was used to generate masks indicating voxels with significant ($p$<0.05) correlation between susceptibility and 18F-Flutemetamol-SUVR.

[*]corresponding author: Jiri van Bergen, Institute for Regenerative Medicine (IREM), University of Zurich, Minervastrasse 145, CH-8032 Zurich, Switzerland, Switzerland +41-44-3891-453, jiri.vanbergen@uzh.ch.



**Competing Financial Interests statement**

Dr. Peter van Zijl is a paid lecturer for Philips Healthcare and is the inventor of technology that is licensed to Philips. This arrangement has been approved by The Johns Hopkins University in accordance with its Conflict of Interest policies. Dr. Paul G. Unschuld is supported by a GE Healthcare grant for investigator initiated research. This funding is in accordance with guidelines issued by the University of Zurich.

We found a bilateral pattern of clusters characterized by a statistical relationship between magnetic susceptibility and 18F-Flutemetamol-SUVR, indicating local correlations between iron and β-amyloid plaque deposition. For two bilateral clusters, located in the frontal and temporal cortex, significant relationships ($p<0.05$) between local β-amyloid and the composite cognitive performance score could be observed. No relationship between whole-cortex β-amyloid plaque load and cognitive performance was observable.

Our data suggest that the local correlation of β-amyloid plaque load and iron deposition may provide relevant information regarding cognitive performance of healthy older adults. Further studies are needed to clarify pathological correlates of the local interaction of β-amyloid, iron and other causes of altered magnetic susceptibility.

## Graphical abstract

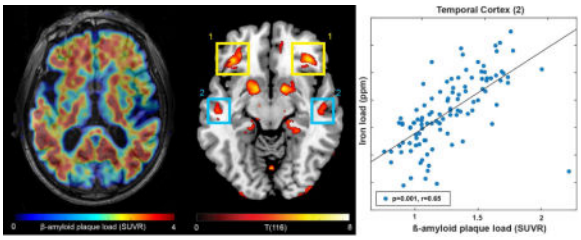


### Keywords

PET; MRI; beta-Amyloid; iron; QSM; aging

## 1 Introduction

The accelerated accumulation of amyloid-beta (Aβ) into β-amyloid plaques is an early observable pathological hallmark of Alzheimer's Disease (AD) (Roberts et al., 2017) and recent studies have demonstrated a close relationship between the individual level of β-amyloid plaque load and increased risk for AD (Jansen et al., 2015; Pietrzak et al., 2015). According to current hypothetical models, Aβ may trigger several downstream pathologies implicated in neurodegeneration, including aggregation of pathological tau, vascular damage and neuroinflammation (Dubois et al., 2016; Jagust et al., 2009; Serrano-Pozo et al., 2016; Sperling et al., 2011). Recent clinical trial data suggest that the therapeutic removal of β-amyloid may prevent cognitive decline if performed early enough (Sevigny et al., 2016). However, novel diagnostic measures are needed to better understand the link between clinically silent AD pathology and initial cognitive changes (Mortamais et al., 2017).

There are a number of clinical studies that demonstrate that the risk for cognitive decline due to AD-pathology is significantly increased by concurrent neurodegeneration (Jagust, 2016; Mormino et al., 2014). Here, iron may provide useful information as recently published studies suggest a link between increased cerebral iron load and AD related cognitive decline (Ayton et al., 2015; Ayton et al., 2017; Kim et al., 2017; van Bergen et al., 2016b). Aβ in its monomeric and aggregated forms can bind iron, resulting in iron accumulation within β-amyloid plaques as well as its conversion from $Fe^{3+}$ into $Fe^{2+}$ (Derry and Kent, 2017;

Everett et al., 2014; Peters et al., 2015). Iron thus may promote local Aβ-related oxidative damage (Andersen et al., 2014; Derry and Kent, 2017; Meadowcroft et al., 2009; Nunomura et al., 2001; Rottkamp et al., 2001) and possibly also trigger ferroptosis (Dixon et al., 2012). Moreover, the process of iron accumulation has been suggested to accelerate the extent and speed of Aβ aggregation into β-amyloid plaques (Everett et al., 2014; Peters et al., 2015). Furthermore, increased iron content is a characteristic of activated microglia in the vicinity of β-amyloid plaques (Zeineh et al., 2015). As activated pro-inflammatory microglia may indicate β-amyloid associated neurodegeneration (Fan et al., 2017; Serrano-Pozo et al., 2016), in vivo measures of iron may be able to infer on these β-amyloid- associated inflammatory processes (Ayton et al., 2017; van Bergen et al., 2016b). Small-vessel cerebrovascular disease (SVCD) is a frequent finding both in AD and in populations at risk for AD, therefore local hemosiderin deposits resulting from vascular leakage may be another cause of local iron accumulation (Guzman et al., 2013; Provenzano et al., 2013; Thal et al., 2014; Young et al., 2008). Recent developments in quantitative susceptibility mapping (QSM) techniques (Deistung et al., 2013a; Li et al., 2011; Lim et al., 2013; Schweser et al., 2012) allow for assessment of relative iron load in vivo.

By using non-invasive susceptibility measures, we and others have recently demonstrated interactions between iron and β-amyloid pathology that may predict longitudinal cognitive performance (Ayton et al., 2017; Derry and Kent, 2017; van Bergen et al., 2016b). However, it remains unclear whether the interaction between iron and β-amyloid might be a whole-cortex or only local effect and if this interaction could be used to infer on the present cognitive status of healthy older adults. Therefore, this cross-sectional study on cognitively healthy older adults aimed to 1) investigate local voxel-level correlations between iron, as measured by QSM, and β- amyloid plaque load, measured by 18F-Flutemetamol-PET; 2) investigate whether susceptibility measures are associated with presence of SVCD, as a potential source of local iron load changes; and 3) determine if iron mediates the effect of β-amyloid plaque load on cognitive performance in cognitively healthy older adults.

## 2 Methods

### 2.1 Participants

For the current study, two cohorts at the Hospital for Psychogeriatric Medicine and Institute for Regenerative Medicine (IREM), University of Zurich (UZH), Switzerland were combined resulting in a total sample of 116 healthy and cognitively unimpaired older participants. Study procedures were in concordance with Human Research Act of Switzerland as well as with the Declaration of Helsinki (World_Medical_Association, 1991). Written informed consent was obtained from all participants before inclusion in the study.

Major inclusion criteria were: preserved everyday functioning and no dementia as assessed by detailed clinical workup under the supervision of a trained physician with experience in dementia diagnostics. Clinical workup considered detailed medical history including psychosocial aspects, the results of a neuropsychological test batteries including the CERAD (Sotaniemi et al., 2012) and the IADL for assessment of self-maintaining and instrumental activities of daily living (Lawton and Brody, 1969).

A composite neuropsychological score was calculated as a combined measure of performance in episodic memory, executive functioning, attention, language and communication. These domains are affected early in individuals suffering from cognitive decline due to AD (Albert et al., 2011). Scores obtained from Verbal Learning and Memory Test (VLMT), Boston Naming Test (BNT), Trail Making Test B/A (TMT), and Stroop Interference Test were converted to z-scores and averaged to generate an equally weighted indicator of cognitive domains. The scores of these specific tests in their respective domains were selected because of their high relative standard deviation, in an effort to increase separation power of the composite score.

Exclusion criteria included: significant medication or drug abuse with possible effects on cognition, inability to partake MRI, MRI scans with the evidence of infection or infarction, clinically relevant changes in red blood cell count, serious medical or neuropsychiatric illness and significant exposure to radiation.

### 2.2 MRI data acquisition

All participants were scanned using a 3T GE SIGNA PET-MR whole-body scanner (GE Medical Systems, Milwaukee, WI, USA) equipped with an 8-channel head coil. T1-weighted brain volume (BRAVO) images (TI=450ms, voxel size=1×1×1$mm^3$, FOV=256×256×256$mm^3$, flip-angle=12°, ASSET factor=2, scan time=6:00min) were acquired for anatomical referencing and automated image segmentation. MR phase measurements used for QSM calculation were acquired using a bipolar multi-echo 3D gradient recalled echo (GRE) sequence with 6 echoes (TR/TE1/ΔTE=40/6/4ms, voxel size=1×1×1$mm^3$, FOV=240×240×140$mm^3$, flip angle=15°, bandwidth=±62.5 kHz, slice and frequency direction flow compensated, ASSET factor=2, phase and slice direction partial Fourier=0.75, scan time=7:53min). Phase data acquired with an echo time in the range of 18-26ms was used for QSM reconstruction (Wu et al., 2012a). Images used to determine WMH were acquired using a CUBE FLAIR sequence and reconstructed with vendor bias field correction (TR=6500ms, TE=134, ARC factor=2, voxel size=0.60×0.49×0.49$mm^3$, FOV=165×250×250$mm^3$ bandwidth=±31.25 kHz, scan time=6:07min).

### 2.3 Effects of structure volume

The T1-weighted image was segmented using a multi-atlas matching approach consisting of 143 Regions of Interest (ROIs) developed as part of the Johns Hopkins University brain atlas. The atlas system is optimized for the parcellation of potential non-healthy brains by applying a Multiple-Atlas Likelihood Fusion algorithm and Ontology Level Control technology on the JHU multi-atlas sets (Djamanakova et al., 2014; Mori et al., 2016; Tang et al., 2013). Specifically, the atlas set of 26 participants aged between 50 and 90 years was used.

To normalize different brain sizes across participants, individual structural volume was corrected with the following approach: *corrected structure volume = original structure volume × (whole sample mean intracranial volume/participant intracranial volume)* (van Bergen et al., 2016b; van Bergen et al., 2017). To investigate possible relationships between structure volume and local β-amyloid plaque load or local iron load, twelve gray- matter

regions of interest were selected from the generated atlas (van Bergen et al., 2017) based on earlier reports on distribution of brain pathology at early stages of AD (Frisoni et al., 2010; Serrano-Pozo et al., 2011). ROI-masks were eroded with two pixels to account for partial volume effects before being used as a mask to analyze average iron load (QSM) and β-amyloid plaque load. For each of the selected ROIs, structure volume was used as outcome variables with local β-amyloid plaque load and local iron load as predictors, respectively.

These and further correlation analyses in this work were corrected for age and gender. False Discovery Rate (FDR) correction for multiple testing (Benjamini and Hochberg, 1995) was applied to all p-values resulting from statistical tests involving multiple comparisons in this work. Input data and residuals were tested for normality using the Shapiro-Wilk test and the homogeneity of data was assessed by Chi-Square testing, if required by the statistical methods. All statistical tests were performed in MATLAB R2016b.

### 2.4 Quantitative susceptibility mapping (QSM) for measuring brain iron load

Multiple processing steps were performed to calculate from the acquired MR phase images the quantitative susceptibility maps of which local cerebral iron load was assessed. First, phase unwrapping was performed using Laplacian-based phase unwrapping (Li et al., 2011). A brain mask was then obtained by skull-stripping the GRE magnitude image acquired at TE of 14ms using FSL's brain extraction tool (BET, FMRIB Oxford, UK). The unwrapped phase images were then divided by $2\pi$*TE to obtain an image of the frequency shift in Hz for each echo. Subsequently, background fields were eliminated with the sophisticated harmonic artifact reduction for phase data (SHARP) (Schweser et al., 2011) approach using a variable spherical kernel size with a maximum radius of 4mm and a regularization parameter of 0.05 (Schweser et al., 2011; Wu et al., 2012b). After removal of background fields, the resulting images of the three echoes were averaged on a pixel-by-pixel basis to obtain a higher SNR as compared to single echo reconstruction (Wu et al., 2012a). Inverse dipole calculations to obtain the susceptibility maps were performed using an iLSQR-based minimization (Li et al., 2015). The average susceptibility of the deep frontal white matter was used as the susceptibility reference for each participant. For clarity and consistency with earlier studies, changes in susceptibility values relative to the reference will be referred to as changes in iron load, due to the previously demonstrated correlation of susceptibility values with tissue iron load in brain gray matter (Deistung et al., 2013a; Li et al., 2011; Lim et al., 2013; Schweser et al., 2012).

### 2.5 Flutemetamol-PET for estimation of brain β-amyloid plaque load

Flutemetamol-PET was used to estimate individual local brain β-amyloid plaque load (Vandenberghe et al., 2010). Individual dose of 140MBq of Flutemetamol was injected into the cubital vein. Time-of-flight algorithms including necessary corrections were applied to reconstruct the PET-images. Standard MRAC images were used to derive attenuation correction maps according standard manufacturer implemented algorithms. Late frame (minutes 85-105) values were standardized by the cerebellar gray matter value (Vandenberghe et al., 2010), resulting in 3D-volumes of Flutemetamol retention as an estimate of β-amyloid plaque load via standard uptake value ratios (SUVR) (matrix=256×256×89, voxel size=1.2×1.2×2.78mm$^3$).

### 2.6 Biological Parametric Mapping (BPM)

To normalize the QSM and PET data of all participants to MNI space a multi-atlas matching approach developed as part of the Johns Hopkins University brain atlas was used. The atlas system is optimized for the parcellation of potential non-healthy brains by applying a Multiple-Atlas Likelihood Fusion algorithm and Ontology Level Control technology on the JHU multi-atlas sets (Djamanakova et al., 2014; Mori et al., 2016; Tang et al., 2013). To limit the analysis to gray matter, a mask was generated by combing all gray matter areas defined by the atlas. The images were smoothed using a 4 mm FWHM Gaussian kernel limited to the gray matter mask in SPM12 (http://www.fil.ion.ucl.ac.uk/spm/software/spm12) running under MATLAB R2016b (Mathworks, Natick, MA). The normalized PET and QSM images and the mask were then used as inputs for the Robust Biological Parametric Mapping toolbox (https://www.nitrc.org/projects/rbpm/) (Casanova et al., 2007; Yang et al., 2011) running under MATLAB R2010a. The BPM toolbox has proven itself as a useful tool to investigate multimodal voxel level correlations while correcting for non-imaging regressors, using the general linear model (GLM) approach (Yang et al., 2011; Zheng et al., 2013). The analysis was performed using robust Huber regression analysis and correcting for age and gender. The result maps were tested for significance using a positive sign T-test, selecting voxels where p-FDR-corrected<0.05 with a cluster threshold of 100 voxels. Subsequently, the significance testing was repeated using a negative sign T-test to investigate potential negative correlations.

### 2.7 Assessment of SVCD by semi-automated WMH detection

To assess occurrence of WMH as an indicator of the overall extend of SVCD and related iron depositions, a semi-automated analysis method was developed that is described in our previous work (van Bergen et al., 2017). In short, each participant's FLAIR images were segmented into gray matter and major white matter regions using the previously generated atlas. The WMH in each white matter region were automatically identified by segmenting and grouping voxels with intensities 1.5 standard deviation above the average gray matter intensity of each participant (Iorio et al., 2013). Automatically segmented regions were then manually validated after which the SVCD burden was inferred on by summing the number of regions exhibiting WMH.

### 2.8 Whole-cortex and local-effects analysis

Single measures of individual cortical ("whole-cortex") β-amyloid plaque load and iron load were calculated for each participant based on average gray-matter ROI values of 18F-Flutemetamol-SUVR and susceptibility, respectively, as reported earlier (van Bergen et al., 2017). Masks of the clusters resulting from the BPM analysis were used to extract the iron load changes and β-amyloid plaque load of each cluster. To identify "amyloid- positive" ($A\beta+$) or "amyloid-negative" ($A\beta-$) status based on single measures and "local" gray matter 18F- Flutemetamol-SUVR values, the cutoff value of 1.562 was used (Vandenberghe et al., 2010). For each cluster, the combined neuropsychological score was compared between $A\beta+$ and $A\beta-$ using a 1-way multivariate analysis of covariance (MANCOVA) with age and years of education as covariates. In a subsequent, secondary analysis, APOE4 carriers and non-carriers were investigated separately.

To test the interaction of SVCD and iron load, the whole-cortex and regional iron load was correlated with the WMH-score.

### 2.9 Region of interest based analysis

The procedure was repeated using ROI masks of the previously mentioned twelve gray matter regions, to investigate region specific β-amyloid plaque load effects on cognitive performance, independent of BPM analysis results. In addition, to investigate potential interplay between the investigated measures a multiple linear regression model with the composite cognitive performance score as outcome and age, gender, APOE4 status, regional iron load and regional β-amyloid plaque load as predictors was used.

## 3 Results

### 3.1 Characteristics of the studied populations and neuropsychological performance

Demographic information for the investigated study population and neuropsychological test performance at time of inclusion are summarized in Table 1. Clinical examination revealed self-reliance and absence of cognitive impairment for all participants. Out of the 116 participants, 24 were APOE4 carriers (22%).

### 3.2 Effects on structure volume

Significant negative correlation between structure volume and local β-amyloid plaque load was found in the globus pallidus ($p=0.002$, Table 2). None of the cortical or memory regions showed significant correlations of volume with iron load or β-amyloid plaque load.

### 3.3 Biological Parametric Mapping (BPM)

Examples of representative 18F-Flutemetamol SUVR images and QSM images can be seen in Figure 1. The BPM analysis of correlation between iron load (susceptibility) and β-amyloid plaque load (18F-Flutemetamol- SUVR) resulted in 37 clusters of at least 100 voxels with p-FDR-corrected<0.05. Graphical representation of the clusters is shown in Figure 2 projected onto a 3D brain and on two exemplary axial slices. Additional axial slices throughout the whole brain can be seen in supplementary Figure 1. Alternatively, the number of significant voxels in brain regions are listed in supplementary Table 1, using the coarse region separation of the Hammers maximum probability atlas (Hammers et al., 2003). The strongest correlations were found in the basal ganglia structures such as globus pallidus ($p=0.001$, $r=0.61$), caudate nucleus ($p=0.001$, $r=0.52$) and putamen ($p=0.002$, $r=0.48$). Many clusters were bilateral in nature and no differences were observed in number or size of clusters between hemispheres. Evaluating the BPM results using a negative sign T-test did not result in significant correlation clusters larger than the 100 voxel threshold.

### 3.4 Whole-cortex and local cluster-effects analysis

The cutoff for 18F-Flutemetamol-SUVR (Vandenberghe et al., 2010) identified 18 participants (16%) “amyloid- positive” ($A\beta+$) and 98 “amyloid-negative” ($A\beta-$) based on whole-cortex β-amyloid plaque load. The Aβ+ participants that were identified using whole-

cortex β-amyloid plaque load did not perform significantly worse than the Aβ− participants on the cognitive performance score (Figure 3A).

Out of the 37 clusters identified using the BPM analysis, two bilateral clusters in the frontotemporal cortex showed significantly lower cognitive performance scores in the Aβ+ group, when categorization in Aβ+ versus Aβ− was made by applying the Flutemetamol-SUVR cutoff to local-cluster β-amyloid plaque load (clusters indicated in Figure 2B). In the frontal cortex cluster eight participants were classified as $A\beta+$, which exhibited significantly lower cognitive performance scores (p=0.012, Figure 3B). Similarly, in the temporal cortex cluster 18 participants were classified as $A\beta+$, which showed significantly lower cognitive performance scores (p=0.049, Figure 3C). In the subsequent analysis, APOE4 status did not split either the whole-cortex or regional β-amyloid plaque load based Aβ+ or Aβ− groups into sub-groups with significant differences between sub- groups. From the bilateral clusters in the frontal and temporal cortex, regional iron load and β-amyloid plaque load measures are shown in Figure 4A and B. The WMH-score did not correlate with whole-cortex iron load or the extracted iron load from the extracted iron load from any of the clusters (p>0.05, examples for two selected clusters in Figure 4C and D). Splitting these correlation analyses by APOE4 status did not result in significant different correlations when using Fisher's r-to-z transformation on the correlation coefficients (Fisher, 1921).

### 3.5 Region of interest based analysis

Composite cognitive performance scores did not differ significantly between $A\beta+$ and $A\beta-$ groups in any of the investigated ROIs (Table 3 and Figure 3A). The multiple linear regression models revealed a negative correlation between β-amyloid plaque load and cognitive performance in the entorhinal cortex and globus pallidus (Table 4). Despite the local correlations between iron load and β-amyloid plaque load found using the BPM analysis, no apparent multicollinearity was observed in any of the ROIs (all variance inflation factors < 2).

## 4 Discussion

In this study we investigated the local correlation between iron- and β-amyloid plaque load, and its potential effect on cognitive performance of healthy old-aged adults. We showed that correlations between iron load and β-amyloid plaques are present in a bilateral pattern that particularly includes clusters located in the frontotemporal cortex and basal ganglia. Moreover, β-amyloid plaque load in frontotemporal clusters was inversely associated with neuropsychological performance. Interestingly, within these clusters, there was no association between SVCD and local susceptibility measures. To our knowledge this is the first study demonstrating that β-amyloid plaque load in brain regions characterized by a local correlation between iron and β-amyloid, relates to cognitive performance levels of healthy, cognitively unimpaired older adults. This local correlation of iron load and β-amyloid plaques is consistent with earlier considerations on iron as a reflection of synergistic pathologies that promote β-amyloid-toxicity in vulnerable brain regions (Ayton et al., 2017; Derry and Kent, 2017; Peters et al., 2015). As these findings were present in a cross-sectional sample, local susceptibility might provide added value for neuroimaging of

prodromal β-amyloid related encephalopathy, reflected by variation of cognitive performance levels.

Earlier studies by Ayton et al. that included longitudinal cognitive performance assessments (Ayton et al., 2015; Ayton et al., 2017; Derry and Kent, 2017) indicate relevance of the association between iron and β-amyloid for cognitive decline and risk for AD. Brain regions affected by the here reported local correlation are consistent with regional effects reported earlier both for iron (Ayton et al., 2017; Cho et al., 2016) and general vulnerability for AD-pathology (Serrano-Pozo et al., 2011).

The relationships of structure volume in globus pallidus with β-amyloid plaque load coincides with a significant effect in the multiple linear regression analysis and with the strongest region of correlation between β-amyloid plaque load and iron load, which was found using the BPM analysis. When the structure volume relationship was not corrected for age, there was a significant negative correlation between iron load and structure volume in the caudate nucleus ($p=0.044$) and putamen ($p=0.031$). This could indicate that both phenomena are synergistically affecting these basal ganglia structures throughout the investigated age range while also affecting cognitive performance. However, it has to be kept in mind that basal ganglia structures are particularly affected by increased iron deposition during aging (Bartzokis et al., 1997; Hallgren and Sourander, 1958). Our observations might also indicate presence of cerebral amyloid angiopathy, which is found frequently in highly perfused brain regions of non-demented elderly individuals (Miller-Thomas et al., 2016), as a source of Aβ and iron deposition. Alternatively, non-specific binding of Flutemetamol in these highly perfused and relatively myelin rich tissues should be considered (Vandenberghe et al., 2010). Therefore, additional studies are needed to characterize the nature of these basal ganglia specific effects.

While only two bilateral regions identified by voxel-level correlation analysis showed the ability to differentiate low cognitive performers, these regions were located in cortical structures commonly affected by AD (Albert et al., 2011; Braak and Braak, 1991). Interestingly, no significant effect on cognition was observable for whole- cortex or ROI-based β-amyloid plaque load in our study, similar to earlier reports of weak associations between β-amyloid plaque load and cognition in cognitively healthy cross-sectional samples (Mortamais et al., 2017). This difference might indicate increased specificity of the BPM analysis for identifying potentially relevant changes, as ROIs were defined in a data-driven approach using statistical tests on the voxel level, rather than predefined anatomical boundaries. Moreover, our finding of significant effects of local β-amyloid in frontotemporal regions of cognitively healthy participants may be consistent with the spatio-temporal spread of disease pathology in neurodegenerative diseases (Brettschneider et al., 2015). As we could observe the effect of β-amyloid on cognition when using iron to define the spatial clusters, processes associated with increased tissue iron might represent mediating factors of β-amyloid plaque effects on cognition. Taking into account that β-amyloid plaque load can be present in cognitively healthy older adults and reflect risk for progression to AD (Jansen et al., 2015), iron load may be a marker for linking β-amyloid plaque load to variation in cognitive performance, and thus may potentially be used to identify subtle dysfunction as very first manifestation of pre- clinical AD (Mortamais et al., 2017). While predictive value

of QSM for cognitive decline has been demonstrated recently (Ayton et al., 2017; Kim et al., 2017), our current findings suggest informative value of local iron for inferring on the relationship between β-amyloid and cognitive performance in a cross-sectional sample. However, as we also find iron-independent effects of β-amyloid on cognitive function, the here reported role of associated tissue iron needs to be interpreted with caution. Our findings of direct relationships between β-amyloid load and cognitive performance in the entorhinal cortex and globus pallidus might be in agreement with the recently proposed concept of in vivo staging based on regional amyloid (Grothe et al., 2017), which does not include effects attributable to local iron. Particularly when considering the broad abundance of ferro-magnetic properties in physiological systems of the human brain, additional characterization of the neurobiological context is a premise for a better understanding of processes potentially associated with increased magnetic susceptibility. Also, generalizability of the here reported effects on cognitive performance may be limited by the size of the study population, which resulted in small case numbers for the β-amyloid positive groups in the ROIs defined by BPM. In addition, the use of the β-amyloid threshold that is defined for whole-cortex applications (Vandenberghe et al., 2010) might not be directly extendable to the specific regions used in this work.

Recent efforts in validation of the QSM technology allow for the in vivo estimation of regional increases of iron (Deistung et al., 2013a; Langkammer et al., 2012) in a context of neurodegenerative disease (Acosta-Cabronero et al., 2013; Ayton et al., 2017; van Bergen et al., 2016a; van Bergen et al., 2016b). When interpreting the susceptibility data, it needs to be considered that the iron load could vary on an intra-voxel basis and that QSM is biased by decreased myelin density (Langkammer et al., 2012; Liu et al., 2011). Myelin loss could be substantial in the deep frontal white matter QSM reference region. Here, myelin loss would increase average susceptibility in the reference region and thus lead to underestimation of the gray matter iron measures. In this study, gray matter regions with low myelin content were investigated, resulting in a negligible contribution of myelin in these regions. In addition, calcifications have been demonstrated to contribute to susceptibility based signals (Deistung et al., 2013b), underlining the heterogeneity of possible causes for altered QSM contrast. The specific MRI hardware setup, sequence parameters and reconstruction algorithms could also affect the results. Specifically, susceptibility contrast could be improved by using longer echo times (Wu et al., 2012a) than the default GE parameters we used for the current study. As these limitations and potential errors were systematic we do not expect them to bias the reported results on differences.

Efforts were made to limit spillover of white matter signal of both QSM and 18F-Flutemetamol-SUVR images by performing the BPM analysis only in the gray matter and selecting only clusters larger than 100 voxels. Optimized normalization to MNI space was performed to assure adequate input to the BPM analysis, but potential effects of the normalization process on the result cannot be fully excluded. Nonetheless, distortion by processes of co-registration of PET with MRI images or bias due to changes occurring in the time between PET and MR acquisition could be avoided as the respective measures were acquired using an integrated PET-MRI.

Interestingly, we found no correlations between iron and SVCD throughout the brain, potentially confirming that the measured iron load is not directly linked to extravasated hemoglobin and vascular pathology. Considering earlier reports on iron containing activated microglia, and microglia as a promoter of β-amyloid plaque toxicity (Serrano-Pozo et al., 2016; Zeineh et al., 2015), local neuroinflammation might be an alternative explanation of our finding of elevated iron in the vicinity of β-amyloid plaques. However, the WMH-score used to infer upon SVCD in the gray matter is only based on occurrence of WMH and not size or specific location. Moreover, as SVCD was only assessed by WMH and no vascular integrity specific imaging was included in the protocol, the fact that no association between iron and vascular disease was found in the current study may be caused by insufficient sensitivity for quantification of vascular disease.

Previous work by us and others did show Aβ-related effects of APOE4 carriers status on iron measures in older populations with advancing cognitive impairment (Ayton et al., 2017; van Bergen et al., 2016b). The fact that in the current study no significant effects of APOE4 were observable is most likely explainable by reduced statistical power due to a low number of APOE4 carriers in the Aβ+ groups. Additionally, the investigated sample showed no signs of cognitive impairment and spanned a large age-range, which could also limit the effects of APOE4 status, as reported earlier (Corrada et al., 2013; Garibotto et al., 2012).

To conclude, in this cross-sectional study we demonstrated a local correlation of markers for iron and β-amyloid plaques, which may characterize brain regions where β-amyloid plaque load inversely relates to individual cognitive performance. While the individual risk for AD dementia has been demonstrated to relate to total β- amyloid plaque load (Pietrzak et al., 2015; Roberts et al., 2017), we here report a potential regional impact of β- amyloid on brain functionality in non-demented older adults, indicated by local correlation with a QSM marker for iron. Further histological and molecular imaging studies are needed to characterize the interplay between iron and various other downstream pathologies that are possibly implicated in conferring local β-amyloid related neuronal damage.

## Supplementary Material

Refer to Web version on PubMed Central for supplementary material.

## Acknowledgments

We thank all participants for their study participation and Esmeralda Gruber for help with patient recruitment and study administration. This work was funded by the Swiss National Science Foundation (Schweizerischer Nationalfonds, SNF), the Mäxi Foundation, the Clinical Research Priority Program (CRPP) of the University of Zurich on Molecular Imaging (MINZ), a grant from the National Institutes of Health (NIBIB) P41 EB015909, investigator initiated research support by GE Healthcare (114-2014-IIR-0075 and 114-2014-IIR-0076), and institutional support from the Institute for Regenerative Medicine (IREM), University of Zurich, Switzerland. This work was supported by the Zurich Impulse Program for the Sustainable Development of Mental Health Services.

## References

Acosta-Cabronero J, Williams GB, Cardenas-Blanco A, Arnold RJ, Lupson V, Nestor PJ. In vivo quantitative susceptibility mapping (QSM) in Alzheimer's disease. PLoS ONE. 2013; 8:e81093. [PubMed: 24278382]

Albert MS, DeKosky ST, Dickson D, Dubois B, Feldman HH, Fox NC, Gamst A, Holtzman DM, Jagust WJ, Petersen RC, Snyder PJ, Carrillo MC, Thies B, Phelps CH. The diagnosis of mild cognitive impairment due to Alzheimer's disease: recommendations from the National Institute on Aging- Alzheimer's Association workgroups on diagnostic guidelines for Alzheimer's disease. Alzheimers Dement. 2011; 7:270–279. [PubMed: 21514249]

Andersen HH, Johnsen KB, Moos T. Iron deposits in the chronically inflamed central nervous system and contributes to neurodegeneration. Cell Mol Life Sci. 2014; 71:1607–1622. [PubMed: 24218010]

Ayton S, Faux NG, Bush AI, Alzheimer's Disease Neuroimaging, I. Ferritin levels in the cerebrospinal fluid predict Alzheimer's disease outcomes and are regulated by APOE. Nat Commun. 2015; 6:6760. [PubMed: 25988319]

Ayton S, Fazlollahi A, Bourgeat P, Raniga P, Ng A, Lim YY, Diouf I, Farquharson S, Fripp J, Ames D, Doecke J, Desmond P, Ordidge R, Masters CL, Rowe CC, Maruff P, Villemagne VL, Salvado O, Bush AI, Life AIB. Cerebral quantitative susceptibility mapping predicts amyloid-beta- related cognitive decline. Brain. 2017; 140:2112–2119. [PubMed: 28899019]

Bartzokis G, Beckson M, Hance DB, Marx P, Foster JA, Marder SR. MR evaluation of age- related increase of brain iron in young adult and older normal males. Magn Reson Imaging. 1997; 15:29–35. [PubMed: 9084022]

Benjamini Y, Hochberg Y. Controlling the False Discovery Rate: A Practical and Powerful Approach to Multiple Testing. 1995:289–300.

Braak H, Braak E. Neuropathological stageing of Alzheimer-related changes. Acta Neuropathol. 1991; 82:239–259. [PubMed: 1759558]

Brettschneider J, Del Tredici K, Lee VM, Trojanowski JQ. Spreading of pathology in neurodegenerative diseases: a focus on human studies. Nat Rev Neurosci. 2015; 16:109–120. [PubMed: 25588378]

Casanova R, Srikanth R, Baer A, Laurienti PJ, Burdette JH, Hayasaka S, Flowers L, Wood F, Maldjian JA. Biological parametric mapping: A statistical toolbox for multimodality brain image analysis. NeuroImage. 2007; 34:137–143. [PubMed: 17070709]

Cho H, Choi JY, Hwang MS, Kim YJ, Lee HM, Lee HS, Lee JH, Ryu YH, Lee MS, Lyoo CH. In Vivo Cortical Spreading Pattern of Tau and Amyloid in the Alzheimer Disease Spectrum. Annals of Neurology. 2016; 80:247–258. [PubMed: 27323247]

Corrada MM, Paganini-Hill A, Berlau DJ, Kawas CH. Apolipoprotein E genotype, dementia, and mortality in the oldest old: the 90+ Study. Alzheimers Dement. 2013; 9:12–18. [PubMed: 23123227]

Deistung A, Schafer A, Schweser F, Biedermann U, Turner R, Reichenbach JR. Toward in vivo histology: a comparison of quantitative susceptibility mapping (QSM) with magnitude-, phase-, and R2*- imaging at ultra-high magnetic field strength. NeuroImage. 2013a; 65:299–314. [PubMed: 23036448]

Deistung A, Schweser F, Wiestler B, Abello M, Roethke M, Sahm F, Wick W, Nagel AM, Heiland S, Schlemmer HP, Bendszus M, Reichenbach JR, Radbruch A. Quantitative susceptibility mapping differentiates between blood depositions and calcifications in patients with glioblastoma. PLoS ONE. 2013b; 8:e57924. [PubMed: 23555565]

Derry PJ, Kent TA. Correlating quantitative susceptibility mapping with cognitive decline in Alzheimer's disease. Brain. 2017; 140:2069–2072. [PubMed: 28899022]

Dixon SJ, Lemberg KM, Lamprecht MR, Skouta R, Zaitsev EM, Gleason CE, Patel DN, Bauer AJ, Cantley AM, Yang WS, Morrison B 3rd, Stockwell BR. Ferroptosis: an iron-dependent form of nonapoptotic cell death. Cell. 2012; 149:1060–1072. [PubMed: 22632970]

Djamanakova A, Tang X, Li X, Faria AV, Ceritoglu C, Oishi K, Hillis AE, Albert M, Lyketsos C, Miller MI, Mori S. Tools for multiple granularity analysis of brain MRI data for individualized image analysis. NeuroImage. 2014; 101:168–176. [PubMed: 24981408]

Dubois, B., Hampel, H., Feldman, HH., Scheltens, P., Aisen, P., Andrieu, S., Bakardjian, H., Benali, H., Bertram, L., Blennow, K., Broich, K., Cavedo, E., Crutch, S., Dartigues, JF., Duyckaerts, C., Epelbaum, S., Frisoni, GB., Gauthier, S., Genthon, R., Gouw, AA., Habert, MO., Holtzman, DM., Kivipelto, M., Lista, S., Molinuevo, JL., O'Bryant, SE., Rabinovici, GD., Rowe, C., Salloway, S.,

Schneider, LS., Sperling, R., Teichmann, M., Carrillo, MC., Cummings, J., Jack, CR, Jr. Preclinical Alzheimer's disease: Definition, natural history, and diagnostic criteria. Alzheimers Dement; Proceedings of the Meeting of the International Working, G., the American Alzheimer's Association on "The Preclinical State of A.D., July; Washington Dc, U.S.A.. 2016. p. 292-323.

Everett J, Cespedes E, Shelford LR, Exley C, Collingwood JF, Dobson J, van der Laan G, Jenkins CA, Arenholz E, Telling ND. Ferrous iron formation following the co-aggregation of ferric iron and the Alzheimer's disease peptide beta-amyloid (1-42). J R Soc Interface. 2014; 11:20140165. [PubMed: 24671940]

Fan Z, Brooks DJ, Okello A, Edison P. An early and late peak in microglial activation in Alzheimer's disease trajectory. Brain. 2017; 140:792–803. [PubMed: 28122877]

Fisher, Ra. On the 'probable error' of coefficient of correlations deduced from a small sample. Metron. 1921; 1:1–32.

Frisoni GB, Fox NC, Jack CR Jr, Scheltens P, Thompson PM. The clinical use of structural MRI in Alzheimer disease. Nat Rev Neurol. 2010; 6:67–77. [PubMed: 20139996]

Garibotto V, Borroni B, Sorbi S, Cappa SF, Padovani A, Perani D. Education and occupation provide reserve in both ApoE epsilon4 carrier and noncarrier patients with probable Alzheimer's disease. Neurol Sci. 2012; 33:1037–1042. [PubMed: 22173784]

Grothe MJ, Barthel H, Sepulcre J, Dyrba M, Sabri O, Teipel SJ, Alzheimer's Disease Neuroimaging, I. In vivo staging of regional amyloid deposition. Neurology. 2017; 89:2031–2038. [PubMed: 29046362]

Guzman VA, Carmichael OT, Schwarz C, Tosto G, Zimmerman ME, Brickman AM, Alzheimer's Disease Neuroimaging, I. White matter hyperintensities and amyloid are independently associated with entorhinal cortex volume among individuals with mild cognitive impairment. Alzheimers Dement. 2013; 9:S124–131. [PubMed: 23375566]

Hallgren B, Sourander P. The effect of age on the non-haemin iron in the human brain. Journal of Neurochemistry. 1958; 3:41–51. [PubMed: 13611557]

Hammers A, Allom R, Koepp MJ, Free SL, Myers R, Lemieux L, Mitchell TN, Brooks DJ, Duncan JS. Three-dimensional maximum probability atlas of the human brain, with particular reference to the temporal lobe. Hum Brain Mapp. 2003; 19:224–247. [PubMed: 12874777]

Iorio M, Spalletta G, Chiapponi C, Luccichenti G, Cacciari C, Orfei MD, Caltagirone C, Piras F. White matter hyperintensities segmentation: a new semi-automated method. Front Aging Neurosci. 2013; 5:76. [PubMed: 24339815]

Jagust W. Is amyloid-beta harmful to the brain? Insights from human imaging studies. Brain. 2016; 139:23–30. [PubMed: 26614753]

Jagust WJ, Landau SM, Shaw LM, Trojanowski JQ, Koeppe RA, Reiman EM, Foster NL, Petersen RC, Weiner MW, Price JC, Mathis CA, Alzheimer's Disease Neuroimaging, I. Relationships between biomarkers in aging and dementia. Neurology. 2009; 73:1193–1199. [PubMed: 19822868]

Jansen WJ, Ossenkoppele R, Knol DL, Tijms BM, Scheltens P, Verhey FR, Visser PJ, Amyloid Biomarker Study, G. Aalten P, Aarsland D, Alcolea D, Alexander M, Almdahl IS, Arnold SE, Baldeiras I, Barthel H, van Berckel BN, Bibeau K, Blennow K, Brooks DJ, van Buchem MA, Camus V, Cavedo E, Chen K, Chetelat G, Cohen AD, Drzezga A, Engelborghs S, Fagan AM, Fladby T, Fleisher AS, van der Flier WM, Ford L, Forster S, Fortea J, Foskett N, Frederiksen KS, Freund-Levi Y, Frisoni GB, Froelich L, Gabryelewicz T, Gill KD, Gkatzima O, Gomez-Tortosa E, Gordon MF, Grimmer T, Hampel H, Hausner L, Hellwig S, Herukka SK, Hildebrandt H, Ishihara L, Ivanoiu A, Jagust WJ, Johannsen P, Kandimalla R, Kapaki E, Klimkowicz-Mrowiec A, Klunk WE, Kohler S, Koglin N, Kornhuber J, Kramberger MG, Van Laere K, Landau SM, Lee DY, de Leon M, Lisetti V, Lleo A, Madsen K, Maier W, Marcusson J, Mattsson N, de Mendonca A, Meulenbroek O, Meyer PT, Mintun MA, Mok V, Molinuevo JL, Mollergard HM, Morris JC, Mroczko B, Van der Mussele S, Na DL, Newberg A, Nordberg A, Nordlund A, Novak GP, Paraskevas GP, Parnetti L, Perera G, Peters O, Popp J, Prabhakar S, Rabinovici GD, Ramakers IH, Rami L, Resende de Oliveira C, Rinne JO, Rodrigue KM, Rodriguez-Rodriguez E, Roe CM, Rot U, Rowe CC, Ruther E, Sabri O, Sanchez-Juan P, Santana I, Sarazin M, Schroder J, Schutte C, Seo SW, Soetewey F, Soininen H, Spiru L, Struyfs H, Teunissen CE, Tsolaki M, Vandenberghe R, Verbeek MM, Villemagne VL, Vos SJ, van Waalwijk van Doorn LJ, Waldemar G, Wallin A,

Wallin AK, Wiltfang J, Wolk DA, Zboch M, Zetterberg H. Prevalence of cerebral amyloid pathology in persons without dementia: a meta-analysis. JAMA. 2015; 313:1924–1938. [PubMed: 25988462]

Kim HG, Park S, Rhee HY, Lee KM, Ryu CW, Rhee SJ, Lee SY, Wang Y, Jahng GH. Quantitative susceptibility mapping to evaluate the early stage of Alzheimer's disease. NeuroImage: Clinical. 2017

Langkammer C, Schweser F, Krebs N, Deistung A, Goessler W, Scheurer E, Sommer K, Reishofer G, Yen K, Fazekas F, Ropele S, Reichenbach JR. Quantitative susceptibility mapping (QSM) as a means to measure brain iron? A post mortem validation study. NeuroImage. 2012; 62:1593–1599. [PubMed: 22634862]

Lawton MP, Brody EM. Assessment of older people: self-maintaining and instrumental activities of daily living. Gerontologist. 1969; 9:179–186. [PubMed: 5349366]

Li W, Wang N, Yu F, Han H, Cao W, Romero R, Tantiwongkosi B, Duong TQ, Liu C. A method for estimating and removing streaking artifacts in quantitative susceptibility mapping. NeuroImage. 2015; 108:111–122. [PubMed: 25536496]

Li W, Wu B, Liu C. Quantitative susceptibility mapping of human brain reflects spatial variation in tissue composition. NeuroImage. 2011; 55:1645–1656. [PubMed: 21224002]

Lim IA, Faria AV, Li X, Hsu JT, Airan RD, Mori S, van Zijl PC. Human brain atlas for automated region of interest selection in quantitative susceptibility mapping: application to determine iron content in deep gray matter structures. NeuroImage. 2013; 82:449–469. [PubMed: 23769915]

Liu C, Li W, Johnson GA, Wu B. High-field (9.4 T) MRI of brain dysmyelination by quantitative mapping of magnetic susceptibility. NeuroImage. 2011; 56:930–938. [PubMed: 21320606]

Meadowcroft MD, Connor JR, Smith MB, Yang QX. MRI and histological analysis of beta- amyloid plaques in both human Alzheimer's disease and APP/PS1 transgenic mice. J Magn Reson Imaging. 2009; 29:997–1007. [PubMed: 19388095]

Miller-Thomas MM, Sipe AL, Benzinger TL, McConathy J, Connolly S, Schwetye KE. Multimodality Review of Amyloid-related Diseases of the Central Nervous System. Radiographics. 2016; 36:1147–1163. [PubMed: 27399239]

Mori S, Wu D, Ceritoglu C, Li Y, Kolasny A, Vaillant MA, Faria AV, Oishi K, Miller MI. MRICloud: Delivering High-Throughput MRI Neuroinformatics as Cloud-Based Software as a Service. Computing in Science & Engineering. 2016; 18:21–35.

Mormino EC, Betensky RA, Hedden T, Schultz AP, Amariglio RE, Rentz DM, Johnson KA, Sperling RA. Synergistic effect of beta-amyloid and neurodegeneration on cognitive decline in clinically normal individuals. JAMA Neurol. 2014; 71:1379–1385. [PubMed: 25222039]

Mortamais M, Ash JA, Harrison J, Kaye J, Kramer J, Randolph C, Pose C, Albala B, Ropacki M, Ritchie CW, Ritchie K. Detecting cognitive changes in preclinical Alzheimer's disease: A review of its feasibility. Alzheimers Dement. 2017; 13:468–492. [PubMed: 27702618]

Nunomura A, Perry G, Aliev G, Hirai K, Takeda A, Balraj EK, Jones PK, Ghanbari H, Wataya T, Shimohama S, Chiba S, Atwood CS, Petersen RB, Smith MA. Oxidative damage is the earliest event in Alzheimer disease. Journal of neuropathology and experimental neurology. 2001; 60:759–767. [PubMed: 11487050]

Peters DG, Connor JR, Meadowcroft MD. The relationship between iron dyshomeostasis and amyloidogenesis in Alzheimer's disease: Two sides of the same coin. Neurobiology of Disease. 2015; 81:49–65. [PubMed: 26303889]

Pietrzak RH, Lim YY, Ames D, Harrington K, Restrepo C, Martins RN, Rembach A, Laws SM, Masters CL, Villemagne VL, Rowe CC, Maruff P, Australian Imaging, B., Lifestyle Research, G. Trajectories of memory decline in preclinical Alzheimer's disease: results from the Australian Imaging, Biomarkers and Lifestyle Flagship Study of ageing. Neurobiol Aging. 2015; 36:1231–1238. [PubMed: 25585532]

Provenzano FA, Muraskin J, Tosto G, Narkhede A, Wasserman BT, Griffith EY, Guzman VA, Meier IB, Zimmerman ME, Brickman AM, Alzheimer's Disease Neuroimaging, I. White matter hyperintensities and cerebral amyloidosis: necessary and sufficient for clinical expression of Alzheimer disease? JAMA Neurol. 2013; 70:455–461. [PubMed: 23420027]

Roberts BR, Lind M, Wagen AZ, Rembach A, Frugier T, Li QX, Ryan TM, McLean CA, Doecke JD, Rowe CC, Villemagne VL, Masters CL. Biochemically-defined pools of amyloid-beta in sporadic Alzheimer's disease: correlation with amyloid PET. Brain. 2017

Rottkamp CA, Raina AK, Zhu X, Gaier E, Bush AI, Atwood CS, Chevion M, Perry G, Smith MA. Redox-active iron mediates amyloid-beta toxicity. Free Radic Biol Med. 2001; 30:447–450. [PubMed: 11182300]

Schweser F, Deistung A, Lehr BW, Reichenbach JR. Quantitative imaging of intrinsic magnetic tissue properties using MRI signal phase: an approach to in vivo brain iron metabolism? NeuroImage. 2011; 54:2789–2807. [PubMed: 21040794]

Schweser F, Sommer K, Deistung A, Reichenbach JR. Quantitative susceptibility mapping for investigating subtle susceptibility variations in the human brain. NeuroImage. 2012; 62:2083–2100. [PubMed: 22659482]

Serrano-Pozo A, Betensky RA, Frosch MP, Hyman BT. Plaque-Associated Local Toxicity Increases over the Clinical Course of Alzheimer Disease. Am J Pathol. 2016; 186:375–384. [PubMed: 26687817]

Serrano-Pozo A, Frosch MP, Masliah E, Hyman BT. Neuropathological alterations in Alzheimer disease. Cold Spring Harb Perspect Med. 2011; 1:a006189. [PubMed: 22229116]

Sevigny J, Chiao P, Bussiere T, Weinreb PH, Williams L, Maier M, Dunstan R, Salloway S, Chen T, Ling Y, O'Gorman J, Qian F, Arastu M, Li M, Chollate S, Brennan MS, Quintero-Monzon O, Scannevin RH, Arnold HM, Engber T, Rhodes K, Ferrero J, Hang Y, Mikulskis A, Grimm J, Hock C, Nitsch RM, Sandrock A. The antibody aducanumab reduces Abeta plaques in Alzheimer's disease. Nature. 2016; 537:50–56. [PubMed: 27582220]

Sotaniemi M, Pulliainen V, Hokkanen L, Pirttila T, Hallikainen I, Soininen H, Hanninen T. CERAD-neuropsychological battery in screening mild Alzheimer's disease. Acta Neurol Scand. 2012; 125:16–23. [PubMed: 21198445]

Sperling RA, Aisen PS, Beckett LA, Bennett DA, Craft S, Fagan AM, Iwatsubo T, Jack CR Jr, Kaye J, Montine TJ, Park DC, Reiman EM, Rowe CC, Siemers E, Stern Y, Yaffe K, Carrillo MC, Thies B, Morrison-Bogorad M, Wagster MV, Phelps CH. Toward defining the preclinical stages of Alzheimer's disease: recommendations from the National Institute on Aging-Alzheimer's Association workgroups on diagnostic guidelines for Alzheimer's disease. Alzheimers Dement. 2011; 7:280–292. [PubMed: 21514248]

Tang X, Oishi K, Faria AV, Hillis AE, Albert MS, Mori S, Miller MI. Bayesian Parameter Estimation and Segmentation in the Multi-Atlas Random Orbit Model. PLoS ONE. 2013; 8:e65591. [PubMed: 23824159]

Thal DR, Attems J, Ewers M. Spreading of Amyloid, Tau, and Microvascular Pathology in Alzheimer's Disease: Findings from Neuropathological and Neuroimaging Studies. Journal of Alzheimers Disease. 2014; 42:S421–S429.

van Bergen JM, Hua J, Unschuld PG, Lim IA, Jones CK, Margolis RL, Ross CA, van Zijl PC, Li X. Quantitative Susceptibility Mapping Suggests Altered Brain Iron in Premanifest Huntington Disease. AJNR Am J Neuroradiol. 2016a; 37:789–796. [PubMed: 26680466]

van Bergen JM, Li X, Hua J, Schreiner SJ, Steininger SC, Quevenco FC, Wyss M, Gietl AF, Treyer V, Leh SE, Buck F, Nitsch RM, Pruessmann KP, van Zijl PC, Hock C, Unschuld PG. Colocalization of cerebral iron with Amyloid beta in Mild Cognitive Impairment. Sci Rep. 2016b; 6:35514. [PubMed: 27748454]

van Bergen JMG, Li X, Quevenco FC, Gietl AF, Treyer V, Leh SE, Meyer R, Buck A, Kaufmann PA, Nitsch RM, van Zijl PCM, Hock C, Unschuld PG. Low cortical iron and high entorhinal cortex volume promote cognitive functioning in the oldest-old. Neurobiology of Aging. 2017

Vandenberghe R, Van Laere K, Ivanoiu A, Salmon E, Bastin C, Triau E, Hasselbalch S, Law I, Andersen A, Korner A, Minthon L, Garraux G, Nelissen N, Bormans G, Buckley C, Owenius R, Thurfjell L, Farrar G, Brooks DJ. 18F-flutemetamol amyloid imaging in Alzheimer disease and mild cognitive impairment: a phase 2 trial. Ann Neurol. 2010; 68:319–329. [PubMed: 20687209]

World_Medical_Association. Declaration of Helsinki. Law Med Health Care. 1991; 19:264–265. [PubMed: 11642954]

Wu B, Li W, Avram AV, Gho SM, Liu C. Fast and tissue-optimized mapping of magnetic susceptibility and T2* with multi-echo and multi-shot spirals. NeuroImage. 2012a; 59:297–305. [PubMed: 21784162]

Wu B, Li W, Guidon A, Liu C. Whole brain susceptibility mapping using compressed sensing. Magn Reson Med. 2012b; 67:137–147. [PubMed: 21671269]

Yang X, Beason-Held L, Resnick SM, Landman BA. Biological parametric mapping with robust and non-parametric statistics. Neuroimage. 2011; 57:423–430. [PubMed: 21569856]

Young VG, Halliday GM, Kril JJ. Neuropathologic correlates of white matter hyperintensities. Neurology. 2008; 71:804–811. [PubMed: 18685136]

Zeineh MM, Chen Y, Kitzler HH, Hammond R, Vogel H, Rutt BK. Activated iron-containing microglia in the human hippocampus identified by magnetic resonance imaging in Alzheimer disease. Neurobiology of Aging. 2015; 36:2483–2500. [PubMed: 26190634]

Zheng W, Nichol H, Liu S, Cheng YCN, Haacke EM. Measuring iron in the brain using quantitative susceptibility mapping and X-ray fluorescence imaging. NeuroImage. 2013; 78:68–74. [PubMed: 23591072]

## Highlights

- Voxel-wise correlation of quantitative susceptibility with β-amyloid by PET-MRI.
- Quantitative susceptibility mapping (QSM) as a measure of local iron deposition.
- 18F-Flutemetamol SUVR for estimating regional distribution of β-amyloid plaques.
- Brain regions of interest were defined by local correlation of iron and β-amyloid.
- Correlating β-amyloid and iron may inform on cognitive performance at high age.

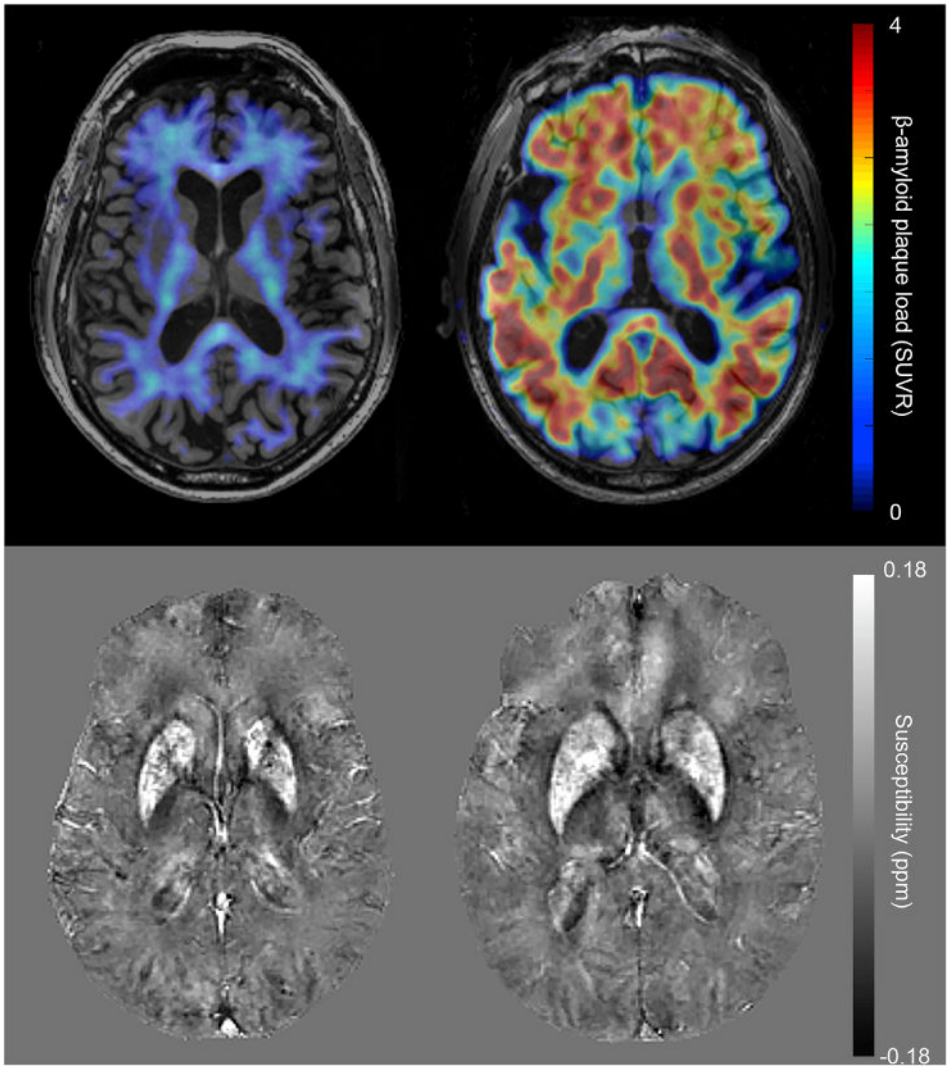


**Figure 1.**

Example images of Aβ− (left) and Aβ+ (right) participants. The top row shows 18F-Flutemetamol SUVR images, in which the Aβ− participant exhibits mostly non-specific white matter uptake while the Aβ+ participant has high β-amyloid plaque load throughout all gray matter regions. The bottom row shows the identical slice in the QSM maps of these participants.

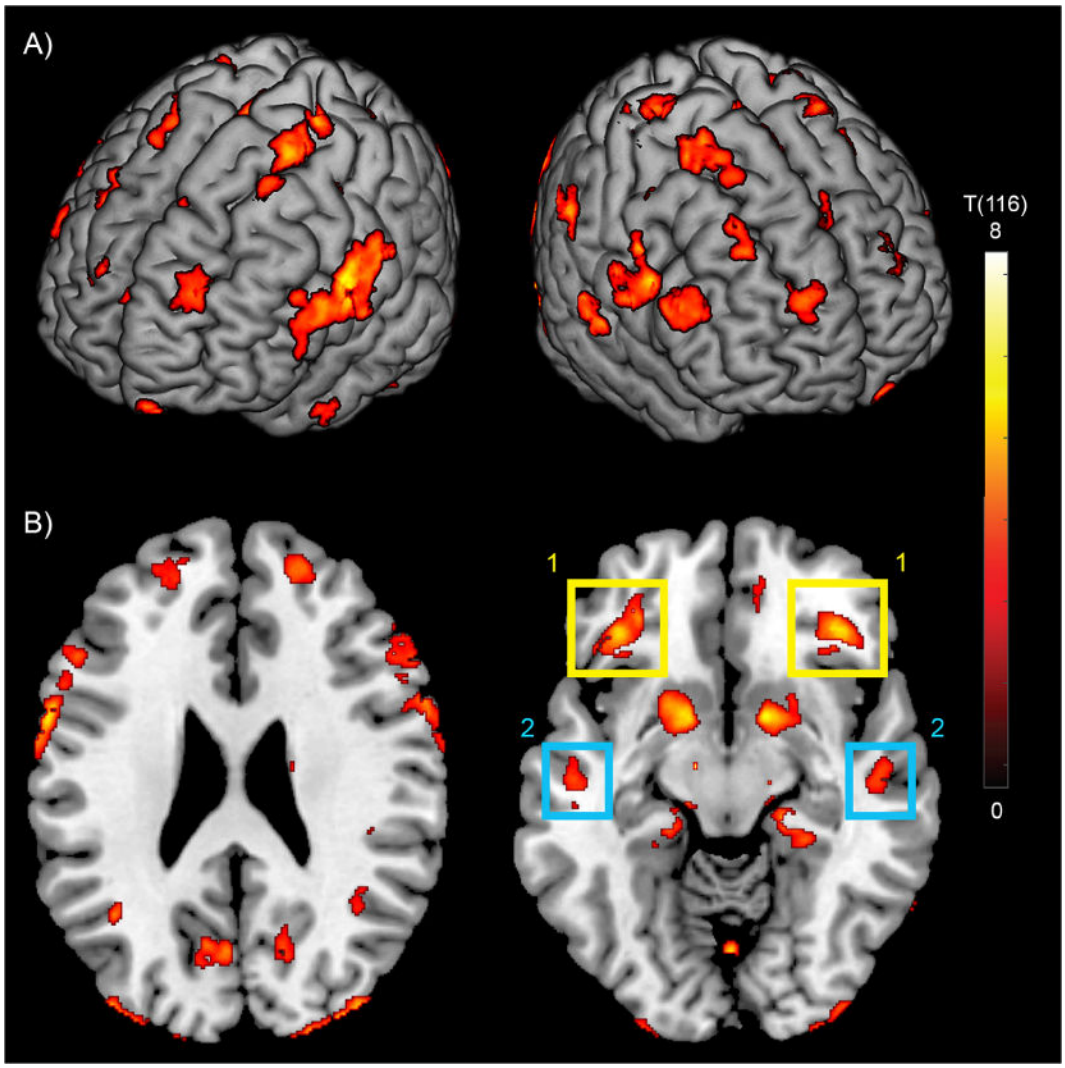


**Figure 2.**

Overlay of regions with significant correlation between iron load (susceptibility) and β-amyloid plaque load (18F-Flutemetamol-SUVR) with p-FDR-corrected<0.05 and a cluster-threshold of 100 voxels, on a 3D brain (A) and on two exemplary slices (B). Extracted β-amyloid plaque load of regions (1) and (2) indicated in (B) identifies Aβ+ with significantly lower cognitive performance compared to Aβ− participants.

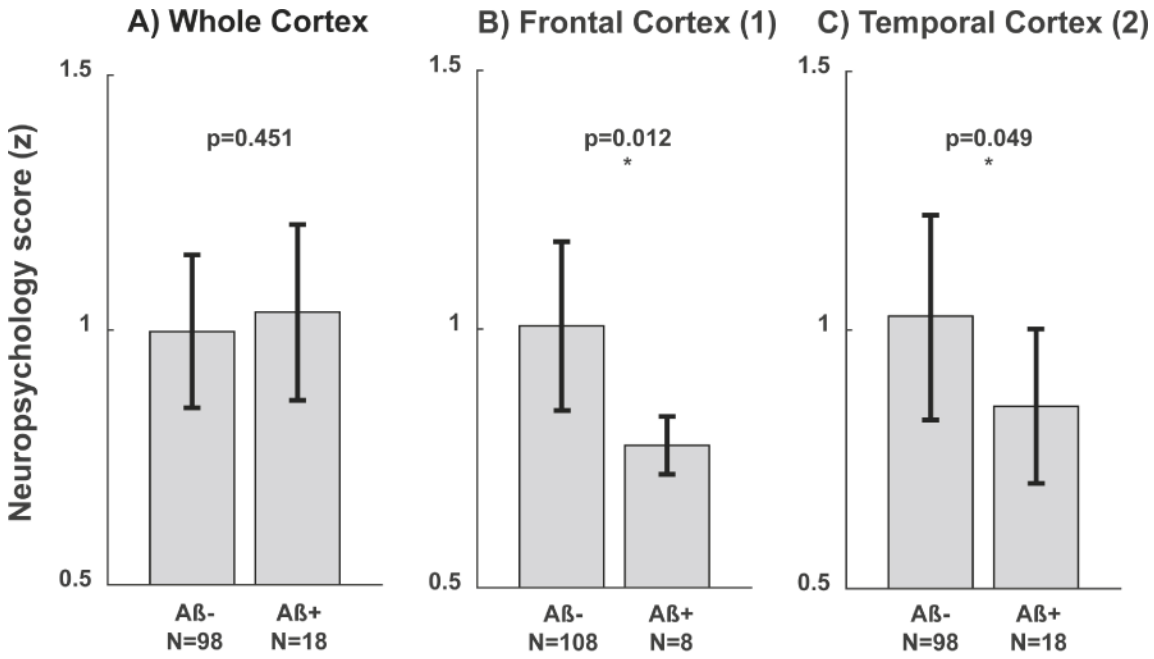


**Figure 3.**

Cognitive performance score for participants grouped as Aβ+ or Aβ− based on the β-amyloid plaque load (18F-Flutemetamol-SUVR) in the (A) whole-cortex, (B) frontal cortex cluster and (C) temporal cortex. * = $p < 0.05$. Error bars represent standard deviation from the mean.

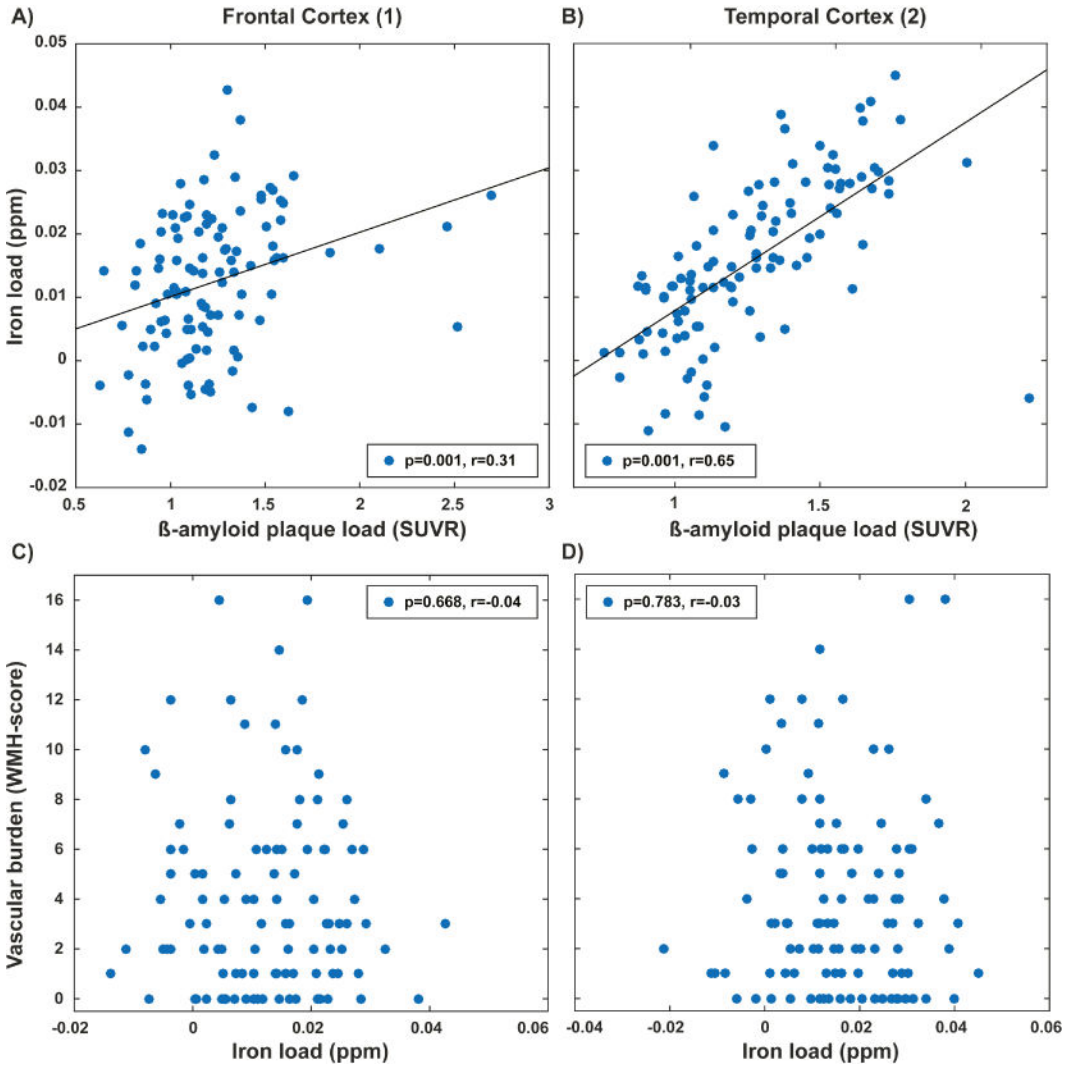


**Figure 4.**

Extracted iron load (susceptibility) and β-amyloid plaque load (18F-Flutemetamol-SUVR) for (A) frontal cortex cluster and (B) temporal cortex clusters found using BPM analysis. Non-significant correlation between vascular burden and iron load in (C) frontal cortex cluster and (D) temporal cortex clusters.

**Table 1**

Overview of sample A) demographics and B) neuropsychological test performance measures as mean ± STD.

| | |
|---|---|
| ***A) Demographics*** | |
| N (M/F) | 116 (69/47) |
| Age (min-max) | 74.81 ± 7.52 (51-95) |
| Education | 15.28 ± 2.76 |
| ApoE-e4 carriers | 26 (22%) |
| Whole-cortex β-amyloid plaque load (SUVR) | 1.28 ± 0.32 |
| Amyloid-positive | 18 (16%) |
| ***B) Neuropsychology*** | |
| MMSE | 28.99 ± 1.10 |
| Boston Naming Test | 2.56 ± 0.75 |
| Trail making test B/A | 2.63 ± 1.26 |
| VLMT: Delayed recall | 8.51 ± 4.04 |
| CERAD: Word list recall | 7.32 ± 1.61 |
| CERAD: Word list learning | 8.31 ± 1.13 |
| CERAD: Fluency | 21.78 ± 6.34 |
| Stroop Interference: color-word | 31.90 ± 11.53 |

## Table 2

Regional correlation analysis for structure volume with the local β-amyloid plaque load and iron load.

| **Correlation of structure size with:** | **β-amyloid plaque load** | ***Iron load*** |
|---|---|---|
| Amygdala | p=0.221 r=0.17 | p=0.780 r=−0.07 |
| Hippocampus | p=0.819 r=0.03 | p=0.209 r=0.17 |
| Entorhinal Cortex | p=0.813 r=0.05 | p=0.214 r=−0.17 |
| Post Cingulate | p=0.822 r=0.04 | p=0.967 r=0.01 |
| Thalamus | p=0.804 r=−0.06 | p=0.374 r=−0.13 |
| Caudate | p=0.821 r=−0.02 | p=0.209 r=−0.19 |
| Putamen | p=0.529 r=−0.11 | p=0.211 r=−0.18 |
| Globus Pallidus | p=0.002 r=−0.36 * | p=0.956 r=−0.03 |
| Frontal Cortex | p=0.426 r=0.13 | p=0.963 r=0.02 |
| Temporal Cortex | p=0.094 r=0.19 | p=0.784 r=0.08 |
| Parietal Cortex | p=0.799 r=−0.06 | p=0.212 r=−0.17 |
| Occipital Cortex | p=0.821 r=0.02 | p=0.957 r=0.03 |

* indicates a significant correlation with $p < 0.05$;

**Table 3**

Cognitive performance score (NPSY, score ± STD) for Aβ− and Aβ+ subjects based on local (ROI) β-amyloid plaque load.

| | Aβ− | | Aβ+ | | |
|---|---|---|---|---|---|
| | **N** | **NPSY** | **N** | **NPSY** | **p** |
| Amygdala | 83 | 1.02 ± 0.16 | 33 | 0.99 ± 0.15 | 0.104 |
| Hippocampus | 83 | 1.01 ± 0.16 | 33 | 1.00 ± 0.17 | 0.987 |
| Entorhinal Cortex | 110 | 1.01 ± 0.16 | 6 | 0.92 ± 0.22 | 0.291 |
| Post Cingulate | 79 | 1.00 ± 0.15 | 37 | 1.01 ± 0.18 | 0.968 |
| Thalamus | 26 | 1.04 ± 0.05 | 90 | 1.00 ± 0.16 | 0.961 |
| Caudate | 99 | 1.01 ± 0.16 | 17 | 0.96 ± 0.18 | 0.296 |
| Putamen | 75 | 1.00 ± 0.13 | 41 | 1.00 ± 0.17 | 0.982 |
| Globus Pallidus | 0 | – | 116 | 1.00 ± 0.16 | – |
| Frontal Cortex | 94 | 1.00 ± 0.16 | 22 | 1.00 ± 0.19 | 0.985 |
| Temporal Cortex | 96 | 1.01 ± 0.15 | 20 | 0.97 ± 0.20 | 0.495 |
| Parietal Cortex | 94 | 1.01 ± 0.15 | 22 | 0.98 ± 0.19 | 0.567 |
| Occipital Cortex | 96 | 1.02 ± 0.16 | 20 | 0.94 ± 0.17 | 0.082 |
| Whole Cortex | 98 | 1.00 ± 0.16 | 18 | 1.02 ± 0.17 | 0.382 |

**Table 4**

Multiple linear regression with cognitive performance as outcome and age, gender, APOE4 status, regional iron load and regional β-amyloid plaque load as predictors.

| | Amygdala | | Hippocampus | | Entorhinal Cortex | | Post Cingulate | | Thalamus | | Caudate | |
|---|---|---|---|---|---|---|---|---|---|---|---|---|
| | β | p | β | p | β | p | β | p | β | p | β | p |
| **Age** | 0.001 | 0.277 | 0.000 | 0.889 | 0.001 | 0.278 | 0.001 | 0.429 | 0.001 | 0.516 | 0.001 | 0.670 |
| **Gender** | −0.005 | 0.869 | −0.003 | 0.932 | −0.005 | 0.863 | −0.006 | 0.857 | 0.000 | 0.989 | −0.006 | 0.861 |
| **APOE4** | −0.012 | 0.753 | −0.025 | 0.509 | −0.018 | 0.629 | −0.014 | 0.712 | −0.020 | 0.587 | −0.025 | 0.505 |
| **Iron load** | −1.368 | 0.184 | 0.601 | 0.594 | −0.214 | 0.798 | −2.005 | 0.259 | −1.361 | 0.263 | −0.480 | 0.488 |
| **β-amyloid plaque load** | −0.144 | 0.084 | −0.089 | 0.352 | **−0.238** | **0.023** | −0.033 | 0.367 | −0.062 | 0.298 | −0.046 | 0.287 |

| | Putamen | | Globus Pallidus | | Frontal Cortex | | Temporal Cortex | | Parietal Cortex | | Occipital Cortex | |
|---|---|---|---|---|---|---|---|---|---|---|---|---|
| | β | p | β | p | β | p | β | p | β | p | β | p |
| **Age** | 0.001 | 0.435 | 0.002 | 0.189 | 0.001 | 0.450 | 0.001 | 0.458 | 0.001 | 0.540 | 0.001 | 0.520 |
| **Gender** | 0.000 | 0.999 | 0.005 | 0.881 | −0.003 | 0.915 | −0.002 | 0.939 | −0.005 | 0.884 | −0.007 | 0.836 |
| **APOE4** | −0.013 | 0.718 | −0.011 | 0.761 | −0.017 | 0.648 | −0.019 | 0.616 | −0.017 | 0.651 | −0.020 | 0.582 |
| **Iron load** | 0.058 | 0.919 | −0.428 | 0.477 | −1.084 | 0.572 | −0.789 | 0.667 | −0.948 | 0.647 | −1.264 | 0.498 |
| **β-amyloid plaque load** | −0.087 | 0.063 | **−0.146** | **0.008** | −0.042 | 0.323 | −0.058 | 0.278 | −0.060 | 0.197 | −0.046 | 0.506 |

Statistically significant p-values are shown in bold.